VOL. 23, NO. 2, 2024, 92-98
elektrika.utm.my
ISSN 0128-4428

ELEKTRIKA
Journal of Electrical Engineering

Investigating Transmission Coefficients of AB-Stacked Bilayer Graphene Nanoribbons with Varied Edge Configurations

Yuki Wong[1], **Nurul Ezaila Alias**[1], **Tian Swee Tan**[2,3], **Michael Loong Peng Tan**[1*]

[1]Faculty of Electrical Engineering, Universiti Teknologi Malaysia, 81310 Skudai, Johor, Malaysia.
[2]Bioinspired Device and Tissue Engineering Research Group, Department of Biomedical Engineering and Health Sciences, Faculty of Electrical Engineering, Universiti Teknologi Malaysia, 81310 Skudai, Johor, Malaysia.
[3]IJN-UTM Cardiovascular Engineering Centre, Institute of Human Centered Engineering, Universiti Teknologi Malaysia, 81310 Skudai, Johor, Malaysia.

[*]Corresponding author: michael@utm.my

Abstract: In this study, the transmission coefficients of AB-stacked bilayer graphene nanoribbons (AB-BGNRs) with different edge configurations, specifically zigzag and armchair edges, are comprehensively investigated. These coefficients are modeled and simulated using the tight-binding (TB) model and non-equilibrium Green's function (NEGF) formalism. The impact of edge structures on the electronic properties of AB-BGNRs is highlighted, providing insights into their potential applications in nanoelectronics devices. Significant variations between zigzag and armchair-edged bilayer graphene nanoribbons (BGNRs) are demonstrated, emphasizing the importance of edge configuration in device performance. This study contributes to the fundamental understanding of edge effects in bilayer graphene and paves the way for the design of more efficient graphene-based electronic devices.

Keywords: BGNRs, edge configurations, NEGF formalism, transmission coefficients, tight-binding model

Article History: received 26 May 2024; accepted 29 July 2024; published 29 August 2024

1. INTRODUCTION

Graphene, a groundbreaking material, forms the foundation of a new class of nanostructures where conduction occurs in single or few layers of carbon atoms arranged in a hexagonal lattice [1]. Its distinct electronic band structure and quasi-relativistic features have sparked significant interest, offering high carrier density and electronic mobility even at room temperature. With the ability to control carrier density through gate voltage [1], graphene has been proposed as a fundamental component for advanced electronic devices [2], including graphene p-n and p-n-p junctions [3], and transistors [4]. The electronic transport properties of Dirac quasiparticles in graphene have emerged as a focal point in nanomaterial science, condensed matter physics, and nanoelectronics [5]. This interest is driven by the potential applications of graphene in advanced electronic devices [6].

In contrast to monolayer graphene's predominantly linear energy spectrum, bilayer graphene exhibits a quadratic energy spectrum in the low-energy regime [7, 8]. In the context of bilayer graphene having a quadratic energy spectrum in the low-energy regime, this aspect of its electronic structure can affect how electrons move through the material. Specifically, the shape and characteristics of the energy bands in bilayer graphene can influence the transmission of electrons across it. Despite extensive research on monolayer graphene, the unique characteristics of bilayer graphene, especially in AB-stacked configurations, require further investigation due to its distinct electronic properties. This is because bilayer graphene is considered equally important as monolayer graphene for both technological applications and fundamental scientific research [4, 9] due to its distinct electronic properties.

Bilayer graphene features two major edge orientations: armchair and zigzag. These orientations exhibit a 30° rotational symmetry with respect to each other [10]. These orientations are characterized by hexagonal dihedral groups within the unit cell, displaying rotational symmetries equivalent to $\pi/3$. Zigzag-edged AB-stacked bilayer graphene nanoribbons (AB-BGNRs) are characterized by edges where the carbon atoms alternate in a zigzag pattern. Armchair-edged AB-BGNRs have edges that resemble the shape of armchair upholstery, where the carbon atoms form a sawtooth pattern.

Graphene nanoribbons (GNRs), which are narrow strips of graphene, are particularly promising for applications in high-performance transistors and next-generation sensors due to their unique electronic properties and tunable bandgaps. These characteristics make GNRs ideal for creating smaller and more efficient electronic components, potentially revolutionizing the electronics industry. Understanding the transmission coefficients of zigzag and armchair-edged GNRs is crucial as it directly impacts their

performance and can lead to significant advancements in these applications.

However, manipulating GNRs at the atomic level poses significant challenges. Achieving precise edge configurations, such as zigzag and armchair edges [10], requires advanced fabrication techniques. Any defects or irregularities in the edges can significantly alter the electronic properties of GNRs, impacting their performance in devices. In addition, the interactions between layers in bilayer graphene add another layer of complexity, as the positioning of atoms can vary, leading to different electronic characteristics. Comprehensively understanding AB-stacked bilayer graphene poses challenges, particularly regarding the influence of edge configurations, specifically zigzag and armchair configurations [10] on the transmission coefficient and electronic transport properties.

To address these challenges, suitable models must be devised to simulate the atomic structure and predict the electronic properties of GNRs. Existing studies often lack a clear and concise method for constructing Hamiltonians for these systems, essential for accurate modelling and simulation. To tackle these issues, a precise Hamiltonian model will be developed using the nearest-neighbor tight-binding (NNTB) approach, tailored for AB-stacked bilayer graphene with both zigzag and armchair edges. Investigating the impact of edge configurations on the transmission coefficient will be pursued using the non-equilibrium Green's function (NEGF) formalism.

2. METHODOLOGY

2.1 Software Setup

To initiate the software environment for simulating the bilayer graphene system, the MATLAB setup is configured to define all requisite constants essential for the subsequent computations. This includes the charge of an electron ($q = 1.6 \times 10^{-19}C$), the reduced Planck's constant ($\hbar = 1.06 \times 10^{-34}Js$), Planck's constant ($h = 2\pi\hbar$), the electron mass ($m = 9.1 \times 10^{-31}kg$), and an imaginary unit for computational purposes ($zplus = i \times 10^{-3}$). Besides, coupling strength parameters are determined based on the assumption that the interlayer distance between layers is 3.35 angstroms [11-14]. The hopping integrals (γ_0, γ_1, γ_3, and γ_4), are initialized based on prior research findings [14-17]. This comprehensive setup ensures that all necessary constants are accurately defined for subsequent simulations and computations within the MATLAB environment.

2.2 NEGF Setup

The NEGF setup involves the initialization of the Hamiltonian matrix and the construction of the alpha and beta matrices, which are pivotal in elucidating the electronic structure and transport characteristics of the bilayer graphene system. This initialization process is tailored to the chosen bilayer graphene topology, whether zigzag or armchair configuration, to accurately capture the unique properties of the system.

In the NEGF framework, the Hamiltonian matrix serves as the cornerstone, encapsulating the system's quantum mechanical properties and governing its evolution over time. It is encompassed by the energy levels, interactions, and dynamics of the electrons within the bilayer graphene structure. The alpha and beta matrices, derived from the Hamiltonian, play crucial roles in representing the intra-layer and inter-layer interactions, respectively, within the bilayer graphene lattice.

In the context of GNRs, width refers to the number of carbon atom positions across the width of the GNRs. It defines the lateral extent of the structure, indicating how many carbon atoms are present along the width direction of the GNRs. This parameter is crucial as it directly influences the electronic properties, conductance characteristics, and potential applications of graphene-based devices. On the other hand, length refers to the longitudinal dimension of the graphene nanoribbons or bilayer graphene layers. It denotes the number of unit cells or carbon-carbon bonds along the longest axis of the GNRs, typically extending in the direction perpendicular to the width. The length determines the overall size of the structure and can affect properties such as electron mobility, thermal conductivity, and the interaction between layers in bilayer graphene configurations.

Specifically, the alpha matrix is characterized by intra-layer interactions, capturing the hopping integrals between adjacent carbon atoms within each layer. Figure 1 shows the alpha unit cells of AB-BGNRs for zigzag and armchair edges, whereas Equations (1) and (2) show their respective alpha matrices with a width of 1 block per unit cell. Looking into the unit cells of AB-BGNRs, the lower layer lattice points are coloured black and white; the upper layer is coloured black and grey. This colouring scheme is chosen to better distinguish the bottom and upper layers. The black lattice points are known as dimers as the carbon atoms are directly above each other between the top and bottom layers.

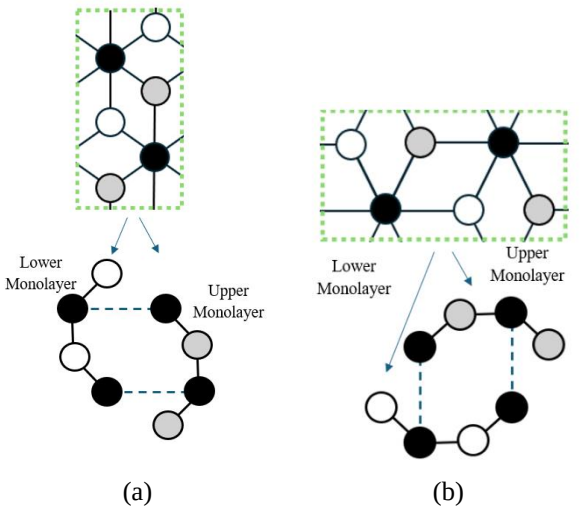

Figure 1. Alpha unit cells of AB-BGNRs for (a) zigzag edge and (b) armchair edge.

$$\alpha = \begin{array}{c} \square \\ l1 \\ l2 \\ l3 \\ l4 \\ u1 \\ u2 \\ u3 \\ u4 \end{array} \begin{array}{c} \begin{array}{cccccccc} l1 & l2 & l3 & l4 & u1 & u2 & u3 & u4 \end{array} \\ \begin{bmatrix} 0 & \gamma_0 & 0 & 0 & \gamma_4 & \gamma_3 & 0 & 0 \\ \gamma_0 & 0 & \gamma_0 & 0 & \gamma_1 & \gamma_4 & 0 & 0 \\ 0 & \gamma_0 & 0 & \gamma_0 & \gamma_0 & \gamma_3 & \gamma_4 & \gamma_3 \\ 0 & 0 & \gamma_0 & 0 & 0 & \gamma_4 & \gamma_1 & \gamma_4 \\ \gamma_4 & \gamma_1 & \gamma_4 & 0 & 0 & \gamma_0 & 0 & 0 \\ \gamma_3 & \gamma_4 & \gamma_3 & \gamma_4 & \gamma_0 & 0 & \gamma_0 & 0 \\ 0 & 0 & \gamma_4 & \gamma_1 & 0 & \gamma_0 & 0 & \gamma_0 \\ 0 & 0 & \gamma_3 & \gamma_4 & 0 & 0 & \gamma_0 & 0 \end{bmatrix} \end{array} \quad (1)$$

$$\alpha = \begin{array}{c} \\ l1 \\ l2 \\ l3 \\ l4 \\ u1 \\ u2 \\ u3 \\ u4 \end{array} \begin{array}{c} \begin{array}{cccccccc} l1 & l2 & l3 & l4 & u1 & u2 & u3 & u4 \end{array} \\ \begin{bmatrix} 0 & \gamma_0 & 0 & 0 & \gamma_4 & \gamma_3 & 0 & 0 \\ \gamma_0 & 0 & \gamma_0 & 0 & \gamma_1 & \gamma_4 & 0 & 0 \\ 0 & \gamma_0 & 0 & \gamma_0 & \gamma_0 & \gamma_3 & \gamma_4 & \gamma_3 \\ 0 & 0 & \gamma_0 & 0 & 0 & \gamma_4 & \gamma_1 & \gamma_4 \\ \gamma_4 & \gamma_1 & \gamma_4 & 0 & 0 & \gamma_0 & 0 & 0 \\ \gamma_3 & \gamma_4 & \gamma_3 & \gamma_4 & \gamma_0 & 0 & \gamma_0 & 0 \\ 0 & 0 & \gamma_4 & \gamma_1 & 0 & \gamma_0 & 0 & \gamma_0 \\ 0 & 0 & \gamma_3 & \gamma_4 & 0 & 0 & \gamma_0 & 0 \end{bmatrix} \end{array} \quad (2)$$

Meanwhile, the beta matrix is delineated by the inter-layer interactions, accounting for the coupling between the top and bottom layers of the bilayer graphene structure. Figure 2 shows the beta unit cells of AB-BGNRs for zigzag edge while Equations (3) shows its respective beta matrix with a width of one block per unit cell.

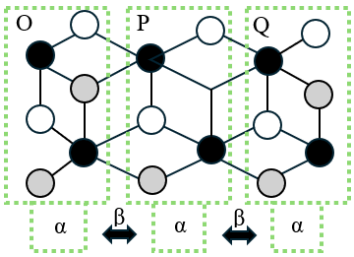

Figure 2. Beta unit cells of AB-BGNRs for zigzag edge.

$$\beta = \begin{array}{c} \\ pl1 \\ pl2 \\ pl3 \\ pl4 \\ pu1 \\ pu2 \\ pu3 \\ pu4 \end{array} \begin{array}{c} \begin{array}{cccccccc} ol1 & ol2 & ol3 & ol4 & ou1 & ou2 & ou3 & ou4 \end{array} \\ \begin{bmatrix} 0 & 0 & 0 & 0 & 0 & 0 & 0 & 0 \\ \gamma_0 & 0 & 0 & 0 & 0 & \gamma_4 & 0 & 0 \\ 0 & 0 & 0 & \gamma_0 & 0 & \gamma_3 & \gamma_4 & 0 \\ 0 & 0 & 0 & 0 & 0 & 0 & 0 & 0 \\ \gamma_4 & 0 & 0 & 0 & 0 & \gamma_0 & 0 & 0 \\ 0 & 0 & 0 & 0 & 0 & 0 & 0 & 0 \\ 0 & 0 & 0 & 0 & 0 & 0 & 0 & 0 \\ 0 & 0 & 0 & \gamma_4 & 0 & 0 & \gamma_0 & 0 \end{bmatrix} \end{array} e^{i\vec{k}(\vec{r_m}-\vec{r_n})} \quad (3)$$

Figure 3 shows the beta unit cells of AB-BGNRs for armchair edge while Equation (4) shows its respective beta matrix with a width of one1 block per unit cell.

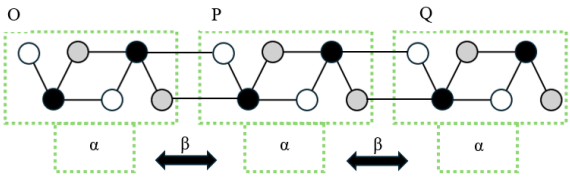

Figure 3. Beta unit cells of AB-BGNRs for armchair edge.

$$\beta = \begin{array}{c} \\ pl1 \\ pl2 \\ pl3 \\ pl4 \\ pu1 \\ pu2 \\ pu3 \\ pu4 \end{array} \begin{array}{c} \begin{array}{cccccccc} ol1 & ol2 & ol3 & ol4 & ou1 & ou2 & ou3 & ou4 \end{array} \\ \begin{bmatrix} 0 & 0 & 0 & \gamma_0 & 0 & 0 & \gamma_4 & \gamma_3 \\ 0 & 0 & 0 & 0 & 0 & 0 & 0 & \gamma_4 \\ 0 & 0 & 0 & 0 & 0 & 0 & 0 & 0 \\ 0 & 0 & 0 & 0 & 0 & 0 & 0 & 0 \\ 0 & 0 & 0 & 0 & 0 & 0 & 0 & \gamma_0 \\ 0 & 0 & 0 & 0 & 0 & 0 & 0 & 0 \\ 0 & 0 & 0 & 0 & 0 & 0 & 0 & 0 \\ 0 & 0 & 0 & 0 & 0 & 0 & 0 & 0 \end{bmatrix} \end{array} e^{i\vec{k}(\vec{r_m}-\vec{r_n})} \quad (4)$$

These matrices are constructed based on the geometric and topological features of the chosen bilayer graphene topology, ensuring an accurate representation of the system's electronic properties including transmission coefficient. Once the alpha and beta matrices have been constructed, they are integrated into the Hamiltonian matrix as submatrices at specified positions, as illustrated in Equation (5), ensuring their proper placement within the complete matrix structure.

$$H = \begin{array}{c} \\ O \\ P \\ Q \end{array} \begin{array}{c} \begin{array}{ccc} O & P & Q \end{array} \\ \begin{bmatrix} \alpha & \beta & 0 \\ \beta' & \alpha & \beta \\ 0 & \beta' & \alpha \end{bmatrix} \end{array} \quad (5)$$

By initializing the Hamiltonian matrix and constructing the alpha and beta matrices in accordance with the chosen bilayer graphene configuration, the NEGF setup establishes the foundation for subsequent quantum mechanical calculations and simulations, enabling comprehensive investigations into the system's transport phenomena. These matrices are essential for describing the transport properties of the system.

2.3 NEGF Calculations

After the Hamiltonian matrices are constructed, the NEGF calculations are set up to determine the transmission coefficient of AB-BGNRs. In NEGF calculations, achieving self-consistency is pivotal for accurately describing the electronic properties of the system, particularly when considering the effects of electron-electron interactions and device-lead coupling. The self-consistent approach involves iteratively solving the equations until a stable solution is reached. Initially, the process involves the setup of an energy grid to cover the desired range of energy values for the calculations. This grid is initialized to ensure that subsequent calculations are performed across a relevant energy spectrum. The convergence criterion is set to 1×10^{-3}, ensuring that the iterative calculations in the NEGF method converge to within a specified tolerance.

Subsequently, the computation proceeds to determine the surface Green's functions associated with the left and right leads of the bilayer graphene device. These surface Green's functions are provided to offer essential insights into the behavior of electrons at the interfaces between the device and its leads, reflecting boundary conditions and interface effects. Following the computation of surface Green's functions, the next step involves the calculation of the self-energy matrices. These matrices, denoted as Σ_1 and Σ_2 are calculated to account for the influence of the device leads on the electronic structure within the device, incorporating effects such as phase-breaking processes and interactions with external environments. Mathematically, the self-energy matrices are illustrated as shown in Equations (6) and (7),

$$\Sigma_1 = \beta^T g_1 \beta \quad (6)$$

$$\Sigma_2 = \beta g_2 \beta^T \quad (7)$$

where g_1 and g_2 are the surface Green's functions associated with the left and right leads, respectively, and β represents the beta matrix.

With the surface Green's functions and self-energy matrices determined, the next step is to compute the total

Green's function of the system, denoted as G. This total Green's function encapsulates the combined effects of the Hamiltonian matrices and the self-energy matrices, providing a comprehensive description of the electronic structure and transport properties within the bilayer graphene device. The total Green's function is determined using Equation (8),

$$G = ((E + zplus)I - H - \Sigma_1 - \Sigma_2 - \Sigma_s)^{-1} \quad (8)$$

where E is the energy, $zplus$ is a small imaginary value to ensure convergence, I is identity matrix, H is the Hamiltonian matrix, and Σ_s represents self-energy contributions from the system, beyond the contacts or leads. The trace operation sums over all electronic states contributing to the transmission process, providing insights into the electron transport characteristics.

The iterative self-consistent loop is then initiated to achieve convergence. In each iteration, the total Green's function is updated to incorporate the effects of the self-energy matrices. Subsequently, the self-energy matrices are recalculated using the updated Green's function. Convergence is assessed by comparing the difference between successive iterations with a predefined convergence criterion. In cases where convergence is not attained, the iteration process is repeated until it is achieved. This approach ensures convergence to a minimum error threshold and has been successfully applied in previous studies [18].

Once self-consistency is established, the converged total Green's function is utilized to calculate the transmission coefficient as a function of energy. Mathematically, the transmission coefficient is given by Equation (9),

$$T(E) = (\Gamma_{left} G \Gamma_{right} G^{\dagger}) \quad (9)$$

where Γ_{left} and Γ_{right} represent the coupling matrices associated with the left and right leads, respectively, and $G^{\dagger}$ denotes the conjugate transpose of G. This transmission coefficient quantifies the probability of an electron incident from one lead transmitting through the device and emerging into the other lead.

Finally, the obtained transmission coefficient data is analyzed and interpreted to elucidate the electronic transport characteristics of AB-BGNRs. The results are evaluated considering the device's geometry, electronic properties, and other relevant parameters to gain insights into electron propagation mechanisms and optimize device performance.

3. RESULTS AND DISCUSSIONS

The transmission coefficient is a crucial metric for two-terminal devices, indicating whether the flux of transmitted travelling waves relative to the incident flux of travelling waves reaches the other side of a potential barrier [19]. In this study, MATLAB is used to plot the transmission coefficient as a function of energy, providing a graphical depiction of the AB-BGNRs' transmission coefficients.

3.1 Transmission Coefficient for Zigzag Edges

The transmission coefficient of the zigzag edge AB-BGNRs is determined using simulations across the entire energy spectrum. A slight dip in the transmission coefficient is observed in the mid-energy band centered around the 0eV region. This transmission coefficient, occasionally exceeding a magnitude of 1, represents the cumulative transmission for all quantum states at a particular energy level and is not normalized to the number of quantum states.

To investigate the effects of varying GNR device widths on the transmission coefficients of zigzag edge AB-BGNRs, simulations are conducted under a fixed length as shown in Figure 4. It is essential to show how increasing the width enhances the transmission coefficient, providing a foundational understanding of the width-dependent behaviour of the system.

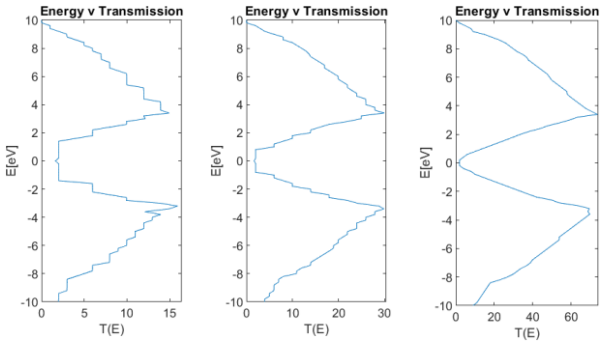

(a) (b) (c)

Figure 4. Transmission plots of AB-BGNRs for increasing widths of (a) 4, (b) 8, and (c) 20 blocks, all with a fixed length of 3 unit cells.

As illustrated in Figure 4, an increase in the device width results in an overall increase in transmission. Figure 4(a) illustrates that the transmission coefficient for a device with a width of 4 blocks per unit cell peaks at 15. In contrast, Figure 4(c) demonstrates that for a device with a width of 20 blocks per unit cell, the transmission coefficient reaches a maximum value of 80. However, it is observed that the mid-band transmission coefficient does not scale proportionally with the peak of the energy spectrum. This finding aligns with previous research [20] indicating that wider nanoribbons tend to have higher transmission coefficients due to increased available quantum states.

To further investigate this phenomenon, the characteristics of carrier energy transmission in the mid-band energy region are examined, particularly around 0 *eV*. Since the transmission coefficient can vary significantly over small energy ranges, especially in systems with complex band structures like bilayer graphene, a finer energy grid is implemented to ensure that all the peaks and troughs of the transmission coefficient are accurately captured, providing a more detailed and precise understanding of the electron transport properties. Figure 5 investigates the effect of varying lengths on the mid-band transmission coefficient for a fixed width of 4 blocks per unit cell.

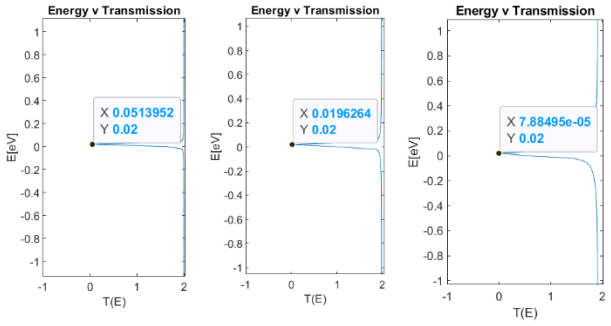

(a) (b) (c)

Figure 5. Mid-band transmission coefficient plots of AB-BGNRs for increasing lengths of (a) 3, (b) 10, and (c) 51 unit cells, all with a fixed width of 4 blocks.

Based on Figure 5, it is observed that increasing the length of the AB-stacked zigzag edge bilayer graphene devices leads to a transition where the mid-band energy transmission decreases towards zero and a non-zero energy band gap starts to emerge, allowing for theoretical engineering of bilayer graphene devices with a non-zero bandgap. This result aligns with the findings in the existing literature [20]. Therefore, it highlights the importance of length in influencing the transmission coefficients and the potential for engineering a zigzag AB-BGNRs with a non-zero bandgap by lengthening the device.

On the other hand, Figure 6 provides a comprehensive view by showing the transmission coefficient for different lengths (3, 10, and 51 unit cells) at a width of 10 blocks per unit cell.

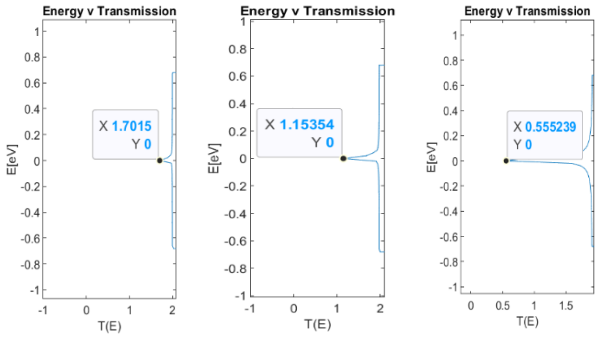

(a) (b) (c)

Figure 6. Mid-band transmission coefficient plots of AB-BGNRs for increasing lengths of (a) 3, (b) 10, and (c) 51 unit cells, all with a fixed width of 10 blocks.

Based on Figure 6, it is important to complement Figure 4 by extending the analysis to a larger width and corroborating the findings that the diminishing mid-band transmission coefficient with increasing lengths is less pronounced for wider devices. It is essential for understanding the interplay between width and length in determining transmission coefficients.

Furthermore, Figure 7 shows the overall transmission coefficient across the entire energy spectrum for varying lengths at a fixed width of 4 blocks per unit cell.

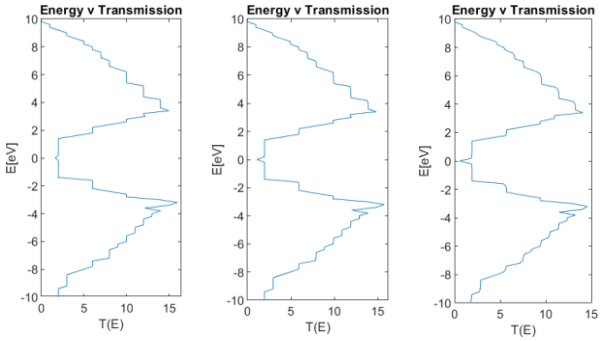

(a) (b) (c)

Figure 7. Transmission plots of AB-BGNRs for the entire energy spectrum with increasing lengths of (a) 3, (b) 10, and (c) 51 unit cells, all with a fixed width of 4 blocks.

Based on Figure 7, it is evident that increasing the length reduces the transmission coefficient across the entire energy spectrum, reinforcing the observations from Figures 4 and 5 and providing a holistic view of the length-dependent transmission coefficients.

3.2 Transmission Coefficient for Armchair Edges

The transmission coefficient across the energy spectrum of the armchair edge AB-BGNRs is computed through simulations for each armchair variant (*3n-1*, *3n*, and *3n+1*). Figure 8 demonstrates the relationship between the width and transmission coefficients across the energy spectrum for different armchair variants. This analysis builds on existing research that has shown the significant impact of edge orientation on electronic properties.

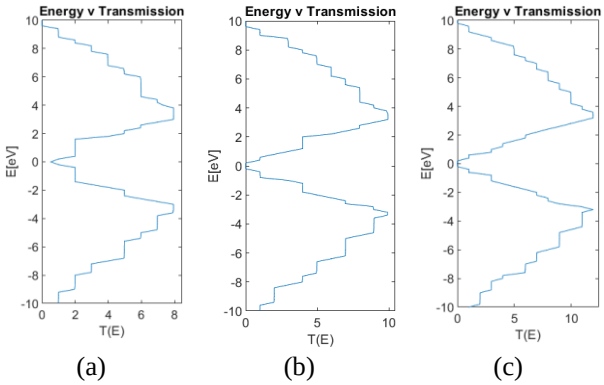

(a) (b) (c)

Figure 8. Transmission plots of AB-BGNRs for different armchair variants with (a) metallic *(3n+1)*, (b) semiconducting *(3n-1)*, and (c) semiconducting *(3n)* variants corresponding to widths 4, 5, and 6 blocks respectively, at a fixed length of 3 unit cells.

Figure 8 shows that the transmission coefficients increase with the width of the device. The transmission coefficient varies between the semiconducting and metallic variants across the energy spectrum. For the metallic variant, the transmission coefficient only approaches zero in the mid-band region. In contrast, for the semiconducting variants, the transmission coefficient is zero in the mid-band region, reflecting the absence of quantum states at those energy eigenvalues. These results are consistent with the characteristics reported in the previous study on armchair graphene nanoribbons [20].

Figure 9 depicts transmission coefficients under increasing widths for each of the armchair variants, enriching the analysis initiated by Figure 8 and contributing to a more comprehensive understanding of transmission coefficients in armchair edge AB-BGNRs.

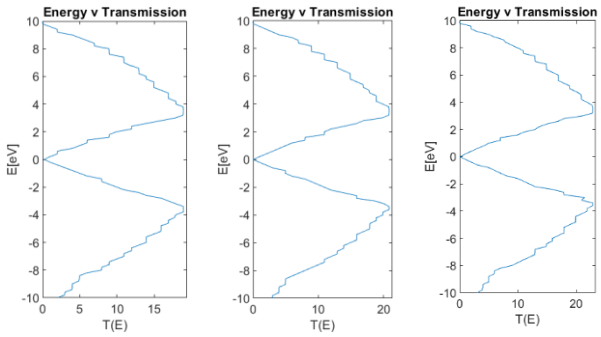

Figure 9. Transmission plots of AB-BGNRs for different armchair variants with (a) metallic *(3n+1)*, (b) semiconducting *(3n-1)*, and (c) semiconducting *(3n)* variants corresponding to widths of 10, 11, and 12 blocks respectively, at a fixed length of 3 unit cells.

Based on Figure 9, it is observed that for the metallic *3n+1* state, the increase in the device width corresponds to a higher transmission coefficient across the energy spectrum, as evidenced by the increase in the maximum value of the transmission coefficient from Figure 8 to Figure 9. Similarly, the increase in the device width also increases the transmission coefficient for the semiconducting variants, as seen in the increase in maximum transmission coefficient value from Figure 8 to Figure 9 for the *3n-1* and *3n* variants respectively. These results are consistent with previous findings on the width dependence of armchair graphene nanoribbons [20].

Similar to the zigzag edge variant, the effects of varying device lengths on the transmission coefficients are investigated with a fixed width. Figure 10 shows the transmission plots for various armchair variants with a fixed length of 51 unit cells. This figure highlights the effect of increasing the device length from 3 unit cells, as shown in Figure 8, to 51 unit cells, demonstrating the impact of length variation on the transmission coefficients across different armchair variants.

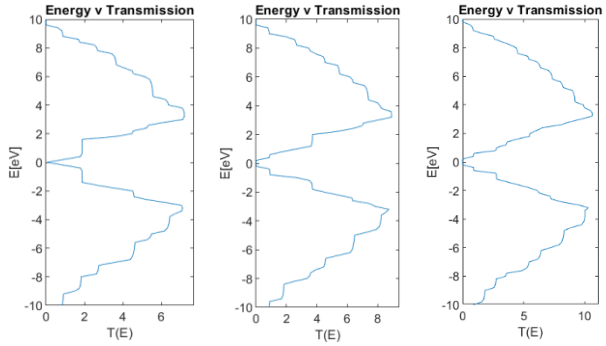

Figure 10. Transmission plots of AB-BGNRs for different armchair variants with (a) metallic *(3n+1)*, (b) semiconducting *(3n-1)*, and (c) semiconducting *(3n)* variants corresponding with widths 4, 5, and 6 blocks respectively, at a fixed length of 51 unit cells.

Based on Figure 10, it is observed that an increase in the device length led to a degradation of the transmission coefficient across the energy spectrum for all the *3n+1*, *3n-1*, and *3n* variants. This quantum result mirrors the macroscopic effect observed in the increase in device resistance with the elongation of the length along the electric field direction or the reduction in device width. This suggests that the quantum simulation results are accurate, as they replicate specific macroscopic effects. This observation aligns with an earlier study on the influence of length on electronic properties of AB-BGNRs [20].

4. CONCLUSION

In this study, the investigation into the transmission coefficients of both zigzag and armchair edge bilayer graphene has provided comprehensive insights into their respective transmission coefficients using the NEGF numerical simulation method with NNTB approximations. For zigzag edges, simulations across varying device dimensions revealed nuanced transmission coefficients, including a slight dip in transmission coefficient in the mid-energy band and the potential for achieving a non-zero bandgap by increasing device length. The inverse relationship between device width and bandgap is underscored, highlighting the importance of carefully selecting dimensions for desired electronic properties. Similarly, for armchair edges, increasing device width corresponded to higher transmission coefficients across the energy spectrum, akin to observations for zigzag edges. A degradation in transmission coefficient is observed with increasing device length. These results align with macroscopic effects, affirming the validity of quantum simulations in capturing real-world transmission phenomena. Overall, these findings offer valuable insights for the design and optimization of bilayer graphene-based devices, particularly in tailoring electronic properties for specific applications in nanoelectronics and beyond.

ACKNOWLEDGMENT

The authors express their deep gratitude for the outstanding support and research-friendly environment offered by Universiti Teknologi Malaysia (UTM). This research received funding from the UTM Fundamental Research (UTMFR) under cost centre number Q.J130000.3823.22H76. The authors also extend their thanks to the Research Management Centre, School of Graduate Studies, and Faculty of Electrical Engineering. Yuki Wong acknowledges the financial assistance provided by the Nexus Young Researcher program at UTM.

REFERENCES

[1] K. S. Novoselov *et al.*, "Two-dimensional gas of massless Dirac fermions in graphene," *nature*, vol. 438, no. 7065, pp. 197-200, 2005.

[2] K. S. Novoselov *et al.*, "Electric field effect in atomically thin carbon films," *science*, vol. 306, no. 5696, pp. 666-669, 2004.

[3] J. González and E. Perfetto, "Critical currents in graphene Josephson junctions," *Journal of Physics: Condensed Matter*, vol. 20, no. 14, p. 145218, 2008.

[4] E. V. Castro *et al.*, "Biased bilayer graphene: semiconductor with a gap tunable by the electric field effect," *Physical review letters*, vol. 99, no. 21, p. 216802, 2007.

[5] N. Tombros, C. Jozsa, M. Popinciuc, H. T. Jonkman, and B. J. Van Wees, "Electronic spin transport and spin precession in single graphene layers at room temperature," *nature*, vol. 448, no. 7153, pp. 571-574, 2007.

[6] A. C. Neto, F. Guinea, N. M. Peres, K. S. Novoselov, and A. K. Geim, "The electronic properties of graphene," *Reviews of modern physics*, vol. 81, no. 1, p. 109, 2009.

[7] O. L. Berman, Y. E. Lozovik, and G. Gumbs, "Bose-Einstein condensation and superfluidity of magnetoexcitons in bilayer graphene," *Physical Review B*, vol. 77, no. 15, p. 155433, 2008.

[8] J. M. Pereira Jr, F. Peeters, and P. Vasilopoulos, "Landau levels and oscillator strength in a biased bilayer of graphene," *Physical Review B*, vol. 76, no. 11, p. 115419, 2007.

[9] J. M. Pereira, P. Vasilopoulos, and F. Peeters, "Tunable quantum dots in bilayer graphene," *Nano letters*, vol. 7, no. 4, pp. 946-949, 2007.

[10] W. Li and R. Tao, "Edge states of monolayer and bilayer graphene nanoribbons," *Journal of the Physical Society of Japan*, vol. 81, no. 2, p. 024704, 2012.

[11] P. Gava, M. Lazzeri, A. M. Saitta, and F. Mauri, "Ab initio study of gap opening and screening effects in gated bilayer graphene," *Physical Review B*, vol. 79, no. 16, p. 165431, 2009.

[12] A. Kuzmenko, I. Crassee, D. Van Der Marel, P. Blake, and K. Novoselov, "Determination of the gate-tunable band gap and tight-binding parameters in bilayer graphene using infrared spectroscopy," *Physical Review B*, vol. 80, no. 16, p. 165406, 2009.

[13] K.-T. Lam and G. Liang, "An ab initio study on energy gap of bilayer graphene nanoribbons with armchair edges," *Applied Physics Letters*, vol. 92, no. 22, 2008.

[14] E. McCann and M. Koshino, "The electronic properties of bilayer graphene," *Reports on Progress in physics*, vol. 76, no. 5, p. 056503, 2013.

[15] M. Chuan *et al.*, "Two-dimensional modelling of uniformly doped silicene with aluminium and its electronic properties," *Advances in nano research*, vol. 9, no. 2, pp. 105-112, 2020.

[16] M. Chuan *et al.*, "Electronic properties of monolayer silicon carbide nanoribbons using tight-binding approach," *Advances in nano research*, vol. 12, no. 2, pp. 213-221, 2022.

[17] H. Raza, *Graphene nanoelectronics: Metrology, synthesis, properties and applications*. Springer Science & Business Media, 2012.

[18] J. C. Slater, "A simplification of the Hartree-Fock method," *Physical review*, vol. 81, no. 3, p. 385, 1951.

[19] V.-N. Do, "Non-equilibrium Green function method: theory and application in simulation of nanometer electronic devices," *Advances in Natural Sciences: Nanoscience and Nanotechnology*, vol. 5, no. 3, p. 033001, 2014.

[20] P. Poobalan, "Tight Binding Model of AB Stacked Bilayer Graphene," 2022.